Published on 13 November 2015. Downloaded by State Public Scientific Technical Library, Siberian Branch of the RAS on 10/19/2020 1:12:47 PM.

Journal of Materials Chemistry C

PAPER

View Article Online
View Journal | View Issue

Cite this: J. Mater. Chem. C, 2015, 3, 12477

Insights into $Ba_4Si_6O_{16}$ structure and photoluminescence tuning of $Ba_4Si_6O_{16}:Ce^{3+},Eu^{2+}$ phosphors

Mingyue Chen,[a] Zhiguo Xia,*[a] Maxim S. Molokeev[bc] and Quanlin Liu[a]

Received 11th October 2015,
Accepted 12th November 2015

DOI: 10.1039/c5tc03271g

www.rsc.org/MaterialsC

The versatile polymorphism and chemical compositions of barium silicates have been studied for a long time and their crystal structures have been established. Herein, we focused on the understanding of the crystal structure of the $Ba_4Si_6O_{16}$ phase and the structural correlation of $Ba_4Si_6O_{16}$ and $Ba_2Si_3O_8$; moreover, the luminescence properties of Ce^{3+},Eu^{2+}-co-activated $Ba_4Si_6O_{16}$ phosphors have been discussed. $Ba_4Si_6O_{16}:Ce^{3+},Eu^{2+}$ phosphors show tunable blue-green emission upon excitation with 365 nm ultraviolet (UV) light. The blue emission originates from Ce^{3+}, whereas the bluish-green emission is ascribed to Eu^{2+}, and variation in the emission peak wavelength from 442 to 497 nm can be achieved by properly tuning the Ce^{3+}/Eu^{2+} ratio. Energy transfer from Ce^{3+} to Eu^{2+} in the $Ba_4Si_6O_{16}$ host has been validated by the variation of emission spectra as well as the variation of Ce^{3+} decay lifetimes with increasing Eu^{2+} concentration, and the energy transfer mechanism is demonstrated to be a resonant type *via* a dipole–dipole process. The results suggest that $Ba_4Si_6O_{16}:Ce^{3+},Eu^{2+}$ phosphors are potential candidates as a blue-green component for UV-excited white light-emitting diodes.

1 Introduction

Recently, in order to fulfil the requirements of white light-emitting diodes (wLEDs), discovery of new/suitable phosphor hosts and the photoluminescence tuning and optimization of the phosphors have drawn much attention from people working in both the academic and industry fields.[1,2] Among them, rare-earth-ion-doped alkaline-earth silicates have been widely investigated due to the versatility in their crystal structures, their adjustable abilities to incorporate rare-earth and transition-metal ions as luminescent centres, their high thermal stability and ease of fabrication, and the wide availability of inexpensive raw materials.[3,4] In particular, barium silicates are of great interest for practical luminescent host materials; a BaO–SiO_2 binary phase diagram focusing on barium silicates with different chemical compositions, such as Ba_2SiO_4, $Ba_2Si_3O_8$, $BaSiO_3$, $Ba_5Si_8O_{21}$, $Ba_3Si_5O_{13}$, Ba_3SiO_5 and $BaSi_2O_5$, is given in Fig. 1.[5] These different barium silicate phases can be obtained through controlling the molar ratio of Ba/Si. Moreover, the sintering temperature can also induce phase transformation. For example, the inset of Fig. 1 exhibits a magnified region highlighting the chemical composition and transition temperature for $Ba_2Si_3O_8$, $Ba_5Si_8O_{21}$, $Ba_3Si_5O_{13}$ and $BaSi_2O_5$. Since the temperatures are very close to each other, phase transitions can easily occur among the four compounds. These barium silicates are good scintillator host candidates since they have congruent melting points.[6]

As is well known, many barium silicate compounds which exist in the above-mentioned BaO–SiO_2 binary phase diagram have been reported as phosphor hosts. Based on a careful paper

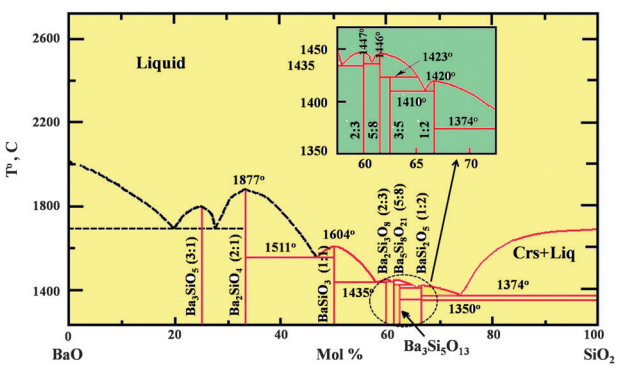

Fig. 1 Schematic phase diagram for the BaO–SiO_2 binary phase system, emphasizing the chemical compositions and existence temperatures of different barium silicate phases; the inset highlights the positions of the stable $Ba_2Si_3O_8$, $Ba_5Si_8O_{21}$, $Ba_3Si_5O_{13}$ and $BaSi_2O_5$ phases.[5]

[a] Key Laboratory of New Energy Materials and Technologies, School of Materials Science and Engineering, University of Science and Technology Beijing, Beijing 100083, China. E-mail: xiazg@ustb.edu.cn; Fax: +86-10-82377955; Tel: +86-10-82377955
[b] Laboratory of Crystal Physics, Kirensky Institute of Physics, SB RAS, Krasnoyarsk 660036, Russia
[c] Department of Physics, Far Eastern State Transport University, Khabarovsk 680021, Russia

Published on 13 November 2015. Downloaded by State Public Scientific Technical Library, Siberian Branch of the RAS on 10/19/2020 1:12:47 PM.

review, the emission of the reported Eu^{2+} single-doped barium silicate phosphors can be tuned from blue to green to yellow light depending on the chemical composition and crystal structure, such as $Ba_5Si_8O_{21}$:Eu^{2+} (λ_{em} = ~480 nm),[6,7] $Ba_2Si_3O_8$($Ba_4Si_6O_{16}$):Eu^{2+} (λ_{em} = ~485 nm),[8,9] Ba_2SiO_4:Eu^{2+} (λ_{em} = 504–510 nm),[10,11] $BaSi_2O_5$:Eu^{2+} (λ_{em} = ~520 nm),[6,12] Ba_3SiO_5:Eu^{2+} (λ_{em} = 504–566 nm or 560–590 nm),[13,14] $BaSiO_3$:Eu^{2+} (λ_{em} = ~550 nm)[15,16] and so on. Among them, Ba_2SiO_4:Eu^{2+} is a well-known green phosphor for wLEDs, but serious luminescent quenching at elevated temperatures restricts its application.[10,11,17,18] Recently, $Sr_xBa_{2-x}SiO_4$:Eu^{2+} was identified to improve thermal stability, with the photoluminescence tuning depending on the Sr/Ba ratio; the intermediate composition with 46% Sr had the highest resistance to thermal quenching.[19] Coordination environment modification belongs to another efficient strategy to tune the emission; it has been found that a small amount of nitrogen can be incorporated into the barium silicate hosts to replace oxygen, since the bonding of Ba–O is relatively weaker than that of Ca–O and Sr–O, which enables nitrogen to more easily replace oxygen in barium silicates.[20] Li *et al.*[20] prepared $Ba_4Si_6O_{16-3x/2}N_x$:Eu^{2+}, and the incorporation of nitrogen (with a maximum solubility of nitrogen at about x = 0.1) could slightly enhance the photoluminescence intensity and quantum efficiency, and further improve the thermal stability. Zhang *et al.*[21] studied Eu^{2+},Ce^{3+}-co-doped $Ba_3Si_5O_{13-\delta}N_\delta$ phosphors with broad emission bands in the range of 400–620 nm; the emission intensity was strongly enhanced by co-doping Ce^{3+} ions into the $Ba_3Si_5O_{13-\delta}N_\delta$:$Eu^{2+}$ *via* energy transfer. Wang *et al.*[22] and Yang *et al.*[23] reported the fluorescence and phosphorescence properties of $Ba_5Si_8O_{21}$:Eu^{2+},Dy^{3+} and $Ba_4(Si_3O_8)_2$:Eu^{2+},Re^{3+} (Re: Dy, Ho), respectively.

Among the reported barium silicate-based phosphors, relatively less research has been carried out on the $Ba_4Si_6O_{16}$ host, and the phase relationship between $Ba_4Si_6O_{16}$ and $Ba_2Si_3O_8$ is also not clear, since both of them have been reported in the references.[8,9,23] In particular, there has been no report on the single-composition emission-tunable phosphor $Ba_4Si_6O_{16}$:Ce^{3+},Eu^{2+} until now. Therefore, in this paper, the crystal structures and luminescence properties of $Ba_4Si_6O_{16}$:Ce^{3+},Eu^{2+} have been investigated in detail. Rietveld refinements were employed to confirm the crystal structure and phase homogeneity. The photoluminescence results reveal that resonance energy transfer can occur from the Ce^{3+} to the Eu^{2+} ions, and that various emission colours of the phosphors from blue through light-blue and finally to bluish-green can be achieved by properly tuning the Ce^{3+}/Eu^{2+} ratio.

2 Experimental section

2.1 Materials and synthesis

The designed samples were synthesized using a conventional solid-state reaction. As starting materials, $BaCO_3$ (A.R.), Li_2CO_3 (A.R.), SiO_2 (A.R.) and the rare-earth dopants CeO_2 and Eu_2O_3 (99.99%) were used as received. Stoichiometric amounts of the reagents were combined and ground together with a small amount of ethanol using an agate mortar and pestle until the mixtures were almost dry (25 min). The charge compensation for the substitution of Ba^{2+} by Ce^{3+} was achieved by adding an equimolar concentration of Li^+. Mixtures were then shifted to the crucible and transferred into the tube furnace to sinter at 1300 °C for 4 h under a reducing atmosphere of N_2–H_2 (5%). The samples were cooled to room temperature in the furnace and were ground again to conduct the following measurements.

2.2 Characterization

The phase structures were investigated using a D8 Advance diffractometer (Bruker Corporation, Germany), operating at 40 kV and 35 mA with Cu Kα radiation (λ = 1.5406 Å). The scanning rate for phase identification was fixed at 8° min^{-1} with a 2θ range from 15° to 60°, and the data for the Rietveld analysis were collected in a step-scanning mode with a step size of 0.02° and 5 s counting time per step over a 2θ range from 5° to 120°.

Photoluminescence emission (PL) and photoluminescence excitation (PLE) spectra were collected using a fluorescence spectrophotometer (F-4600, HITACHI, Japan) equipped with a photomultiplier tube operating at 400 V, and a 150 W xenon lamp as the excitation source. The luminescence decay curves were obtained using a FLSP-920 fluorescence spectrophotometer (Edinburgh Instruments Ltd, UK), and an nF900 flash lamp was used as the excitation source. The internal quantum efficiency was measured using the integrated sphere on the same FLSP-920 instrument, and white $BaSO_4$ powder was used as a reference to measure the absorption.

3 Results and discussion

3.1 Insight into the $Ba_4Si_6O_{16}$ structure

Filipenko *et al.* firstly reported the crystal structure of the synthetic barium silicate $Ba_4Si_6O_{16}$.[24] However, as for the chemical composition and crystal structure of the $Ba_4Si_6O_{16}$ phase, previous reports mentioned the $Ba_2Si_3O_8$, $Ba_4Si_6O_{16}$ and $Ba_4(Si_3O_8)_2$ phases, but there was no discussion on the phase relationship between them, especially $Ba_2Si_3O_8$ and $Ba_4Si_6O_{16}$. According to the data in the JCPDS and ICSD databases, the crystallographic parameters of $Ba_4Si_6O_{16}$ (JCPDS No. 83-1442, ICSD 100310) derived from single crystal data are as follows: a = 12.477, b = 4.685 and c = 13.944 Å, whilst β = 93.54°, with the space group of $P2_1/c$; as a comparison, the crystallographic parameters of $Ba_2Si_3O_8$ (JCPDS 27-1035) originating from powder diffraction are as follows: a = 13.960, b = 4.6895 and c = 12.486 Å, and β = 93.54°, with the space group $P2_1/a$. Seemingly, $Ba_2Si_3O_8$ and $Ba_4Si_6O_{16}$ have different space group symbols with different cell parameters. In fact, $P2_1/a$ is a non-standard setting, and therefore it should be transformed to the standard one by exchanging a and c; the space group will then become $P2_1/c$, and the cell parameters are a = 12.486, b = 4.6895 and c = 13.960 Å, with β = 93.54°. Therefore, it is clear that "$Ba_2Si_3O_8$" and "$Ba_4Si_6O_{16}$" are associated with absolutely the same compound.

In this paper, the crystal structures of the as-prepared $Ba_4Si_6O_{16}$:Ce^{3+} and $Ba_4Si_6O_{16}$:Ce^{3+},Eu^{2+} samples were investigated.

 This journal is © The Royal Society of Chemistry 2015

Published on 13 November 2015. Downloaded by State Public Scientific Technical Library, Siberian Branch of the RAS on 10/19/2020 1:12:47 PM.

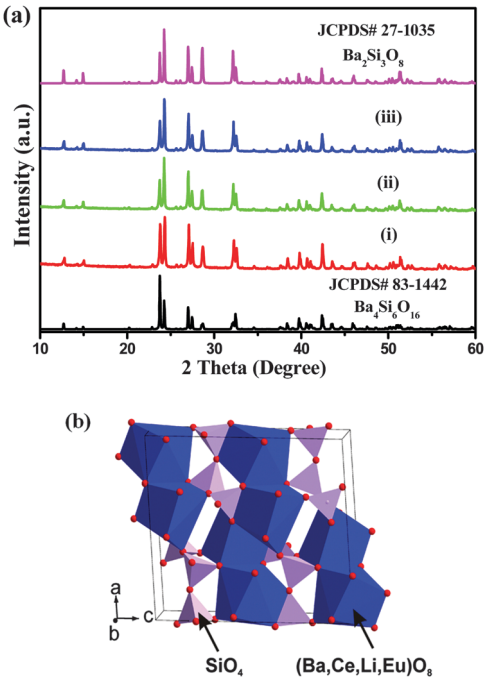

Fig. 2 (a) XRD patterns of as-prepared $Ba_{3.86}Si_6O_{16}$:0.07Ce^{3+},0.07Li^+ (i), $Ba_{3.855}Si_6O_{16}$:0.07Ce^{3+},0.07Li^+,0.005Eu^{2+} (ii) and $Ba_{3.835}Si_6O_{16}$:0.07Ce^{3+},0.07-Li^+,0.025Eu^{2+} (iii). The standard data for $Ba_4Si_6O_{16}$ (JCPDS 83-1442) and $Ba_2Si_3O_8$ (JCPDS 27-1035) are shown as a reference. (b) Representative crystal structure of $Ba_4Si_6O_{16}$, where Ce/Li and Eu occupy the same Ba sites.

Considering that Ce^{3+} ions substitute for Ba^{2+} sites, the co-substitution of Ce^{3+}–Li^+ for two Ba^{2+} should be formed to balance the charge, as mentioned in the experimental section. XRD patterns of as-prepared $Ba_{3.86}Si_6O_{16}$:0.07Ce^{3+},0.07Li^+, $Ba_{3.855}Si_6O_{16}$:0.07Ce^{3+},0.07Li^+,0.005Eu^{2+} and $Ba_{3.835}Si_6O_{16}$:0.07-Ce^{3+},0.07Li^+,0.025Eu^{2+} are comparatively shown in Fig. 2(a), and the standard data for $Ba_4Si_6O_{16}$ (JCPDS 83-1442) and $Ba_2Si_3O_8$ (JCPDS 27-1035) are also shown as a comparison. As is shown in Fig. 2(a), it is clearly found that the crystal structures of $Ba_4Si_6O_{16}$:Ce^{3+} and $Ba_4Si_6O_{16}$:Ce^{3+},Eu^{2+} matched well with that of $Ba_2Si_3O_8$ (JCPDS 27-1035), although the samples were achieved in accordance with the stoichiometric amounts of $Ba_4Si_6O_{16}$, which further verified the same crystal structure for these two chemical formulae. We can see that the intensities of the two powder XRD patterns are different, which may be ascribed to the diverse preferred orientation of the samples. In this paper, we will use the formula $Ba_4Si_6O_{16}$ hereafter for consistency.

The crystal structure of the $Ba_4Si_6O_{18}$ compound is demonstrated in Fig. 2(b). The [SiO_4] tetrahedrons are corner-linked to each other by bridging oxygen atoms to form a Zweier single chain. Three corner-sharing [SiO_4] single chains are linked into a Zweier triple chain in $Ba_4Si_6O_{16}$. In a Zweier single chain, every other tetrahedron is connected with another tetrahedron which lies on a neighbouring Zweier single chain.[22] Based on the consideration of the ionic radius and charge, the doped Ce^{3+}, Li^+ and Eu^{2+} will enter the Ba^{2+} sites, as is also exhibited in Fig. 2(b). In order to further verify such a result, Fig. 3 gives the Rietveld refinement analysis of two selected samples, $Ba_{3.86}Si_6O_{16}$:0.07Ce^{3+},0.07Li^+ and $Ba_{3.845}Si_6O_{16}$:0.07Ce^{3+},0.07-Li^+,0.015Eu^{2+}, respectively, and the main parameters of processing and refinement for the data are shown in Table 1. Almost all the diffraction peaks in Fig. 3 were indexed by a monoclinic cell ($P2_1/c$) with parameters close to those of $Ba_2Si_3O_8$. Therefore, this crystal structure was taken as the starting model for Rietveld refinement. The Ba ion site was occupied by Ce, Li and Eu ions (Fig. 2(b)) with fixed occupations according to the suggested chemical formulae. The refinements were stable and gave low R-factors (Table 1).

3.2 Luminescence properties of Ce^{3+}/Li^+-doped $Ba_4Si_6O_{16}$ phosphors

The photoluminescence excitation and emission spectra of $Ba_4Si_6O_{16}$:Ce^{3+} are shown in Fig. 4(a). The Ce^{3+}-activated $Ba_4Si_6O_{16}$ phosphor exhibits a broad emission band extending from 380 to 650 nm under 365 nm excitation, and the emission peak is located at about 442 nm. Obviously, the observed broad emission band can be ascribed to the transition from the lowest energy crystal field splitting component of the 5d level to the 4f ground state of Ce^{3+} incorporated in the $Ba_4Si_6O_{16}$ host lattice. Monitored at 442 nm, the excitation spectra give two bands with peaks centred at about 305 and 337 nm in the wavelength range of 200–400 nm. Fig. 4(b) gives the PL spectra of $Ba_{3.86-2x}Si_6O_{16}$:$x$$Ce^{3+}$,$x$$Li^+$ at different Ce^{3+} concentrations. It can be seen that the emission spectra consist of an asymmetric broad band centred at 442 nm. The emission intensity firstly increases with increasing Ce^{3+} concentration, and the optimal doping concentration is x = 0.07, then the emission intensity declines dramatically as the content of Ce^{3+} exceeds 0.07 mol, due to

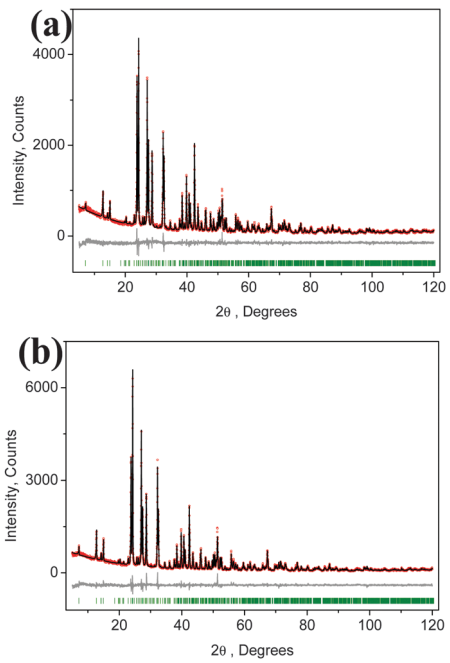

Fig. 3 Difference Rietveld plots of (a) $Ba_{3.86}Si_6O_{16}$:0.07Ce^{3+},0.07Li^+ and (b) $Ba_{3.845}Si_6O_{16}$:0.07Ce^{3+},0.07Li^+,0.015Eu^{2+}.

Published on 13 November 2015. Downloaded by State Public Scientific Technical Library, Siberian Branch of the RAS on 10/19/2020 1:12:47 PM.

Table 1 Main parameters of the processing and refinement for $Ba_{3.86}Si_6O_{16}$:0.07Ce^{3+},0.07Li^+ and $Ba_{3.845}Si_6O_{16}$:0.07Ce^{3+},0.07Li^+,0.015Eu^{2+}

Compound	$Ba_{3.86}Si_6O_{16}$:0.07Ce^{3+},0.07Li^+	$Ba_{3.845}Si_6O_{16}$:0.07Ce^{3+},0.07Li^+,0.015Eu^{2+}
Space group	$P2_1/c$	$P2_1/c$
a, Å	12.4863(2)	12.4859(2)
b, Å	4.6905(1)	4.6904(1)
c, Å	13.9485(3)	13.9498(3)
β, Å	93.566(1)	93.558(1)
V, Å^3	815.33(3)	815.39(3)
Z	2	2
R_{wp}, %	7.95	8.28
R_p, %	6.13	6.38
χ^2	2.25	2.80

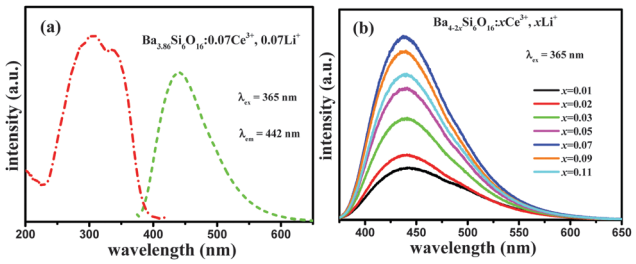

Fig. 4 (a) PLE and PL spectra of $Ba_{3.86}Si_6O_{16}$:0.07Ce^{3+},0.07Li^+; (b) PL spectra of $Ba_{3.86-2x}Si_6O_{16}$:$x$$Ce^{3+}$,$x$$Li^+$ (x = 0.01–0.11).

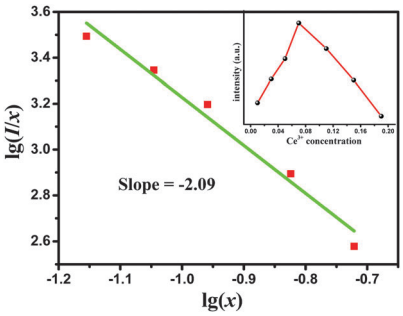

Fig. 5 The relationship of lg(x) *versus* lg(I/x) for $Ba_{3.86-2x}Si_6O_{16}$:$x$$Ce^{3+}$,$x$$Li^+$ phosphors; the inset shows their PL intensities as a function of Ce^{3+} content.

concentration quenching. In general, concentration quenching is mainly caused by non-radiative energy migration among the Ce^{3+} ions at high concentrations. The critical distance between the Ce^{3+} ions can be calculated using the following equation:[25]

$$R_C = 2\left[\frac{3V}{(4\pi X_c Z)}\right]^{1/3}, \quad (1)$$

where V is the volume of the unit cell, Z represents the formula units per unit cell and X_c is the critical concentration. By taking the values of V = 815.33 Å^3, Z = 2 and X_c = 0.07, the critical transfer distance, R_C, was found to be 22.4 Å. There are two types of energy transfer process: one is the exchange interaction, and the other one is the multipolar interaction. In the case of the exchange interaction, the critical distance between the sensitizer and activator is always shorter than 5 Å.[26] Since the critical distance calculated for $Ba_4Si_6O_{16}$:Ce^{3+} is larger than 5 Å, there is little possibility of energy transfer *via* the exchange interaction mechanism. Consequently, it is the electric multipolar interaction that will take place for energy transfer among the Ce^{3+} ions. According to Dexter's theory, there are three types of multipole–multipole interactions: dipole–dipole, dipole–quadrupole and quadrupole–quadrupole, respectively.[27,28] The emission intensity (I) of the multipolar interaction can be determined from the change of the emission intensity from the emitting level with multipolar interaction, which follows eqn (2):[28]

$$\frac{I}{x} = K\left[1 + \beta(x)^{\frac{\theta}{3}}\right]^{-1}, \quad (2)$$

where x is the activator concentration, which is not less than the critical concentration, I/x is the emission intensity (I) per activator concentration (x), K and β are constants for the same excitation condition for a given host crystal and θ is a function of multipole–multipole interaction, taking values of 6 (dipole–dipole), 8 (dipole–quadrupole) or 10 (quadrupole–quadrupole).[28] To get a correct θ value for the two emission centers, the dependence of log(I/x) on log(x) is plotted, which yields a straight line with a slope equal to $-\theta/3$. Because the critical quenching concentration of Ce^{3+}(x) has been determined to be about 0.07 in the $Ba_4Si_6O_{16}$:Ce^{3+} phosphor, I/x is plotted as a function of x for x > 0.07. The dependence of log(I/x) on log(x) is linear in Fig. 5, with a slope of −2.09. Therefore, the value of θ has been calculated to be approximately 6, which indicates that the dipole–dipole interaction is the dominant concentration quenching mechanism of Ce^{3+} emission in the $Ba_4Si_6O_{16}$:Ce^{3+} phosphor.

3.3 Photoluminescence tuning and energy transfer of Eu^{2+}/Ce^{3+}/Li^+-codoped $Ba_4Si_6O_{16}$ phosphors

For comparison, the PLE and PL spectra of $Ba_{3.86}Si_6O_{16}$:0.07Ce^{3+},0.07Li^+, $Ba_{3.975}Si_6O_{16}$:0.025Eu^{2+} and $Ba_{3.855}Si_6O_{16}$:0.07Ce^{3+},0.07Li^+,0.005Eu^{2+} are given in Fig. 6. The PL spectrum of Eu^{2+} singly-doped $Ba_4Si_6O_{16}$ exhibits a broad emission band centred at 497 nm, attributed to the typical $4f^65d^1$–$4f^7$ transition of Eu^{2+}, and the PLE spectrum shows a broad absorption from 230 to 420 nm. As for $Ba_{3.855}Si_6O_{16}$:0.07Ce^{3+},0.07Li^+,0.005Eu^{2+}, the PL spectrum upon excitation at 365 nm exhibits not only the Ce^{3+} emission band at 442 nm but also the Eu^{2+} emission band at 497 nm, so that the observed emission band is very broad, and the PLE spectra of this sample have similar spectral profiles, as shown in Fig. 6(c). These results give strong evidence

 This journal is © The Royal Society of Chemistry 2015

Published on 13 November 2015. Downloaded by State Public Scientific Technical Library, Siberian Branch of the RAS on 10/19/2020 1:12:47 PM.

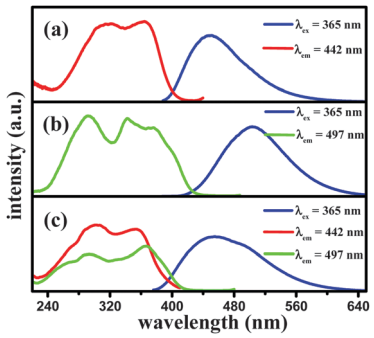

Fig. 6 PLE (left) and PL (right) spectra of $Ba_{3.86}Si_6O_{16}$:0.07Ce^{3+},0.07Li^+ (a), $Ba_{3.975}Si_6O_{16}$:0.025Eu^{2+} (b), and $Ba_{3.855}Si_6O_{16}$:0.07Ce^{3+},0.07Li^+,0.005Eu^{2+} (c).

for the effective Ce^{3+}–Eu^{2+} energy transfer (ET). The occurrence of ET can be clearly understood from noting the spectral overlap between the Ce^{3+} emission band in $Ba_{3.86}Si_6O_{16}$:0.07Ce^{3+},0.07Li^+ and the Eu^{2+} excitation band in $Ba_{3.975}Si_6O_{16}$:0.025Eu^{2+}. A formula for the energy transfer is expressed in the following eqn (3):[29]

$$P_{SA} = 2\pi/h|\langle S, A^*|H_{SA}|S^*, A\rangle|^2 \int_{SA} g_S(E)g_A(E)dE, \qquad (3)$$

where P_{SA} and H_{SA} are the energy transfer rate and interaction Hamiltonian, respectively; the matrix element indicates the interaction between the initial state, $|S^*,A\rangle$, and the final state, $\langle S,A^*|$. The integral represents the spectral overlap between the PL spectrum of sensitizers and the PLE spectrum of activators. As shown in eqn (3), the existing spectral overlap indicates that the energy transfer from Ce^{3+} to Eu^{2+} ions in $Ba_4Si_6O_{16}$ is possible.

In order to study the effect of the doping concentration of Eu^{2+} ions on the luminescence properties of this series of phosphors, PL spectra of $Ba_{3.86-y}Si_6O_{16}$:0.07Ce^{3+},0.07Li^+,yEu^{2+} (y = 0, 0.003, 0.005, 0.007, 0.010, 0.015 and 0.025) with a fixed Ce^{3+} concentration and variable Eu^{2+} concentrations were measured and are shown in Fig. 7(a), and the normalized PL spectra are also given in Fig. 7(b) for comparison. With increasing Eu^{2+} content, y, the emission intensity of Ce^{3+} is reduced, followed by the enhancement of Eu^{2+} emission due to ET from Ce^{3+} to Eu^{2+}. Meanwhile, an obvious red-shift in the emission spectra can be observed from Fig. 7(b), and, consequently, the emission color of the phosphor gradually evolved from blue emission (y = 0) to green emission (y = 0.025).

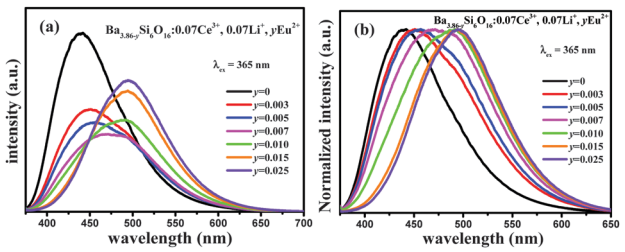

Fig. 7 As-measured (a) and normalized (b) PL spectra of $Ba_{3.86-y}Si_6O_{16}$:0.07Ce^{3+},0.07Li^+,yEu^{2+} (y = 0, 0.003, 0.005, 0.007, 0.010, 0.015 and 0.025) phosphors under 365 nm excitation.

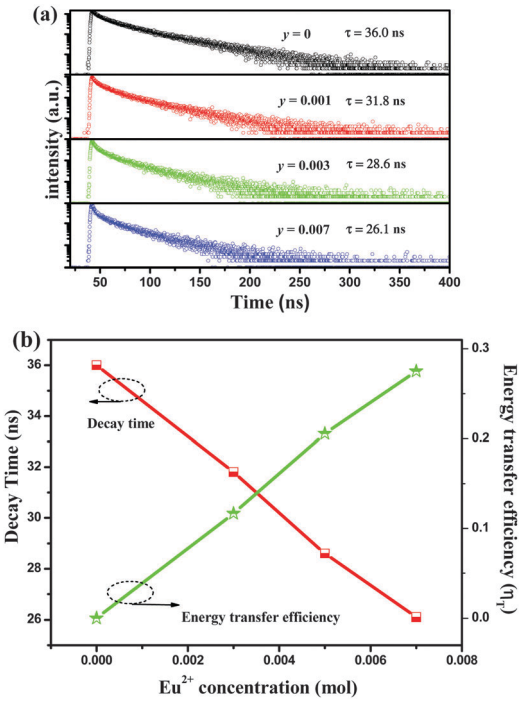

Fig. 8 (a) The decay curves and lifetime values of Ce^{3+} in $Ba_{3.86-y}Si_6O_{16}$:0.07Ce^{3+},0.07Li^+,yEu^{2+} with different Eu^{2+} contents (y): y = 0, 0.001, 0.003 and 0.007. (b) Dependence of the fluorescence lifetime of the Ce^{3+} and energy transfer efficiency on the doped Eu^{2+} molar concentration in $Ba_{3.86-y}Si_6O_{16}$:0.07Ce^{3+},0.07Li^+,yEu^{2+} samples.

To further investigate the dynamic luminescence process between Ce^{3+} and Eu^{2+}, the decay curves of Ce^{3+} for the $Ba_{3.86-y}Si_6O_{16}$:0.07Ce^{3+},0.07Li^+,yEu^{2+} phosphors were measured by monitoring at 442 nm with the excitation at 351 nm, and the measured decay curves are depicted in Fig. 8(a). The decay curve can be well fitted with a second-order exponential decay mode by the use of eqn (4):[30–32]

$$I(t) = A_1 \exp(-t/\tau_1) + A_2 \exp(-t/\tau_2), \qquad (4)$$

where I is the luminescence intensity, A_1 and A_2 are constants, t is the time, and τ_1 and τ_2 are rapid and slow lifetime values for exponential components, respectively. Based on eqn (4), we can collect the A_1, A, τ_1 and τ_2 values based on the fitting of the decay curves. Therefore, the effective lifetime constant (τ^*) can be calculated using eqn (5):

$$\tau^* = (A_1\tau_1^2 + A_2\tau_2^2)/(A_1\tau_1 + A_2\tau_2). \qquad (5)$$

The effective decay time (τ^*) was calculated to be 36.0, 31.8, 28.6 and 26.1 ns for $Ba_{3.86-y}Si_6O_{16}$:0.07Ce^{3+},0.07Li^+,yEu^{2+} with y = 0, 0.001, 0.003 and 0.007, respectively. The energy transfer efficiency (η_T) from the Ce^{3+} to the Eu^{2+} ions can be expressed using eqn (6):[33–35]

$$\eta_T = 1 - (I_S/I_{S0}) = 1 - (\tau_S/\tau_{S0}), \qquad (6)$$

where τ_{S0} and τ_S stand for the lifetimes of Ce^{3+} in the absence and the presence of Eu^{2+}, respectively. With increasing Eu^{2+} concentration, the η_T value is calculated and is shown in Fig. 8(b).

Published on 13 November 2015. Downloaded by State Public Scientific Technical Library, Siberian Branch of the RAS on 10/19/2020 1:12:47 PM.

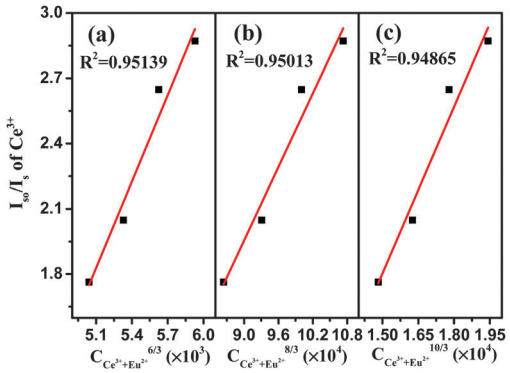

Fig. 9 Dependence of I_{S0}/I_S of Ce^{3+} on $C^{6/3}$ (a), $C^{8/3}$ (b) and $C^{10/3}$ (c).

As seen in Fig. 8(b), the average lifetime decreased monotonically and the energy transfer efficiency increased sharply with increasing Eu^{2+} content. The η_T value reached 27.5% at y = 0.007, which also indicated that the energy transfer efficiency can increase with increasing Eu^{2+} content, as demonstrated in Fig. 8(b).

On the basis of Dexter's energy transfer expressions of multipolar interaction and Reisfeld's approximation, the following relation can be given:[36,37]

$$\eta_{S0}/\eta \propto C^{\alpha/3}; \quad (7)$$

here, C is the total concentration of Ce^{3+} and Eu^{2+}, and η_{S0} and η_S are the luminescence quantum efficiencies of the sensitizer Ce^{3+} in the absence and presence of the activator Eu^{2+}. The values for α = 6, 8 and 10 are ascribed to dipole–dipole, dipole–quadrupole and quadrupole–quadrupole interactions, respectively. However, the value of η_{S0}/η_S is hard to obtain. So, it can be approximately calculated instead of the I_{S0}/I_S, where I_{S0} and I_S are the luminescence intensities of the sensitizer Ce^{3+} in the absence and presence of the activator Eu^{2+} separately. The following relationship can be obtained:[38]

$$I_{S0}/I \propto C^{\alpha/3}. \quad (8)$$

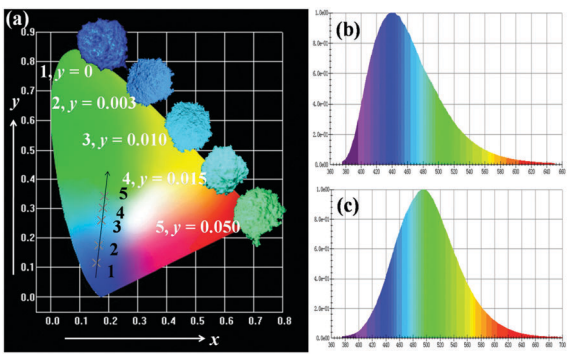

Fig. 10 (a) CIE chromaticity diagram and a series of digital photographs of the selected $Ba_{3.86-y}Si_6O_{16}$:0.07Ce^{3+},0.07Li^+,yEu^{2+} (y = 0, 0.003, 0.010, 0.015 and 0.050) phosphors (λ_{ex} = 365 nm). The magnification of the emission spectra of (b) $Ba_{3.86}Si_6O_{16}$:0.07Ce^{3+},0.07Li^+ and (c) $Ba_{3.835}Si_6O_{16}$:0.07Ce^{3+},0.07Li^+,0.025Eu^{2+}, showing the difference of the emission spectra.

The relationship of $(I_{S0}/I_S) \propto C^{\alpha/3}$ is illustrated in Fig. 9. By consulting the fitting factor R^2, the relation $(I_{S0}/I_S) \propto C^{6/3}$ has the best fitting, implying that the dipole–dipole interaction is applied for the energy transfer from Ce^{3+} to Eu^{2+}.

Fig. 10 shows the chromaticity diagram and a series of digital photographs, upon excitation with the 365 nm UV lamp, of the selected $Ba_{3.86-y}Si_6O_{16}$:0.07Ce^{3+},0.07Li^+,yEu^{2+} (y = 0, 0.003, 0.010, 0.015 and 0.050) phosphors (λ_{ex} = 365 nm). From Fig. 10, one can find out that the emission colours of the $Ba_{3.86-y}Si_6O_{16}$:0.07Ce^{3+},0.07Li^+,yEu^{2+} phosphors can be obviously shifted from blue to bluish-green by adjusting the Eu^{2+} doping level. Accordingly, the corresponding CIE coordinates of $Ba_{3.86-y}Si_6O_{16}$:0.07Ce^{3+},0.07Li^+,yEu^{2+} can be changed from (0.1571, 0.1156) to (0.1790, 0.3023), due to the different compositions of the Ce^{3+} and Eu^{2+} ions. Also, on the right side, one can clearly find the red shift from the representative spectra (Fig. 10(b) and (c)). Based on these results, it is clear that these blue-green $Ba_{3.86-y}Si_6O_{16}$:0.07Ce^{3+},0.07Li^+,yEu^{2+} phosphors can be efficiently excited in the UV range and show tunable emission from blue to green light. Additionally, the internal quantum efficiencies (IQE) of typical samples have been measured by a previously reported method.[39] The corresponding values of the selected $Ba_{3.86-y}Si_6O_{16}$:0.07Ce^{3+},0.07Li^+,yEu^{2+} (y = 0, 0.003, 0.025 and 0.05) phosphors are 35.9%, 39.3%, 41.5% and 63.6%, respectively, and it is found that the value increases with increasing Eu^{2+} content. These results indicate that $Ba_{3.86-y}Si_6O_{16}$:0.07Ce^{3+},0.07Li^+,yEu^{2+} phosphors can act as potential blue-green tunable phosphors for the possible applications in wLEDs.

4 Conclusion

In summary, the $Ba_4Si_6O_{16}$ phase has been identified from the BaO–SiO_2 binary phase diagram, the crystal structure of $Ba_4Si_6O_{16}$ has been analysed *via* the measured XRD patterns and Rietveld refinement, and the phase relationship between $Ba_2Si_3O_8$ and $Ba_4Si_6O_{16}$ has also been investigated. Color-tunable $Ba_4Si_6O_{16}$:Ce^{3+},Eu^{2+} phosphors have been prepared, and the phosphors could be excited by ultraviolet light and show blue bluish-green emission, depending on the concentrations of Ce^{3+} and Eu^{2+}. The energy transfer from Ce^{3+} to Eu^{2+} ions is deduced *via* spectral overlap between the Ce^{3+} PL spectra and Eu^{2+} PLE spectrum, then confirmed by the variation of emission spectra as well as the reduction of Ce^{3+} decay lifetimes with increasing Eu^{2+} concentration. Additionally, the energy transfer mechanism from Ce^{3+} to Eu^{2+} ions is confirmed to be multipolar interaction, according to the discussion of expressions from Dexter and Reisfeld. Generally, these results indicate that $Ba_4Si_6O_{16}$:Ce^{3+},Eu^{2+} phosphors may be promising as candidates for UV-pumped wLEDs.

Acknowledgements

This work was supported by the National Natural Science Foundations of China (Grant No. 51572023 and 51272242), Natural Science Foundations of Beijing (2132050), the Program for New Century Excellent Talents in University of Ministry of

 This journal is © The Royal Society of Chemistry 2015

Published on 13 November 2015. Downloaded by State Public Scientific Technical Library, Siberian Branch of the RAS on 10/19/2020 1:12:47 PM.

Education of China (NCET-12-0950), Beijing Nova Program (Z131103000413047), the Funds of the State Key Laboratory of New Ceramics and Fine Processing, Tsinghua University (KF201306), and Fundamental Research Funds for the Central Universities (FRF-TP-14-005A1).

Notes and references

1 M. M. Shang, C. X. Li and J. Lin, *Chem. Soc. Rev.*, 2014, **43**, 1372–1386.
2 Z. G. Xia, C. G. Ma, M. S. Molokeev, Q. L. Liu, K. Rickert and K. R. Poeppelmeier, *J. Am. Chem. Soc.*, 2015, **13**, 12494.
3 S. H. Miao, Z. G. Xia, M. S. Molokeev, M. Y. Chen, J. Zhang and Q. L. Liu, *J. Mater. Chem. C*, 2015, **3**, 4616.
4 Z. G. Xia, S. H. Miao, M. Y. Chen, M. S. Molokeev and Q. L. Liu, *Inorg. Chem.*, 2015, **54**, 7684.
5 M. E. Huntelaar and E. H. P. Cordfunke, *J. Nucl. Mater.*, 1993, **201**, 250.
6 Y. Eagleman, E. B. Courchesne and S. E. Derenzo, *IEEE Trans. Nucl. Sci.*, 2012, **59**, 479.
7 T. Ishigaki, K. Sato, S. Kamei, K. Uematsu, K. Todaa and M. Sato, *Mater. Res. Soc. Symp. Proc.*, 2012, **1471**, 75.
8 F. Xiao, Y. N. Xue and Q. Y. Zhang, *Spectrochim. Acta, Part A*, 2009, **74**, 758.
9 W. S. Song, H. J. Kim, Y. S. Kim and H. Yang, *J. Electrochem. Soc.*, 2010, **157**, J319.
10 J. K. Han, M. E. Hannah, A. Piquette, J. B. Talbot, K. C. Mishra and J. McKittrick, *J. Lumin.*, 2015, **161**, 20.
11 M. Zhang, J. Wang, Q. H. Zhang, W. J. Ding and Q. Su, *Mater. Res. Bull.*, 2007, **42**, 33.
12 A. Herrmannn, A. Simon and C. Russel, *J. Lumin.*, 2012, **132**, 215.
13 M. Yamaga, Y. Masui and N. Kodama, *Opt. Mater.*, 2014, **36**, 1776.
14 J. K. Park, M. A. Lim, K. J. Choi and C. H. Kim, *J. Mater. Sci.*, 2005, **40**, 2069.
15 Z. G. Cui, G. H. Jia, D. G. Deng, Y. J. Hua, S. L. Zhao, L. H. Huang, H. P. Wang, H. P. Ma and S. Q. Xu, *J. Lumin.*, 2012, **132**, 153.
16 C. F. Guo, Y. Xu, Z. Y. Ren and J. T. Bai, *J. Electrochem. Soc.*, 2011, **158**, J373.
17 X. J. Li, Y. J. Liang, F. Yang, Z. G. Xia, W. Z. Huang and Y. L. Li, *J. Mater. Sci.: Mater. Electron.*, 2013, **24**, 3199.
18 J. S. Kim, Y. H. Park, S. M. Kim, J. C. Choi and H. L. Park, *Solid State Commun.*, 2005, **133**, 445.
19 K. A. Denault, J. Brgoch, M. W. Gaultois, A. Mikhailovsky, R. Petry, H. Winkler, S. P. DenBaars and R. Seshadri, *Chem. Mater.*, 2014, **26**, 2275.
20 Y. Q. Li, Y. Fang, N. Hirosaki, R. J. Xie, L. H. Liu, T. Takeda and X. Y. Li, *Materials*, 2010, **3**, 1692.
21 R. L. Zhang, T. Maeda, R. Maruta, S. Kusaka, B. J. Ding, K. Murai and T. Moriga, *J. Solid State Chem.*, 2010, **183**, 620.
22 P. J. Wang, X. H. Xu, D. C. Zhou, X. Yu and J. B. Qiu, *Inorg. Chem.*, 2015, **54**, 1690.
23 Z. F. Yang, Y. H. Hu, L. Chen and X. J. Wang, *Opt. Mater.*, 2013, **35**, 1264.
24 O. S. Filipenko, E. A. Pobedimskaya, V. I. Ponomarev and N. V. Belov, *Phys.-Dokl.*, 1971, **16**, 77.
25 G. Blasse, *J. Solid State Chem.*, 1986, **62**, 207.
26 G. Blasse and B. C. Grabmaier, *Luminescent Materials*, Springer, Berlin, 1994.
27 L. Ozawa and P. M. Jaffe, *J. Electrochem. Soc.*, 1971, **118**, 1678.
28 L. G. Van Uitert, *J. Electrochem. Soc.*, 1967, **114**, 1048.
29 C. H. Hsu, B. M. Cheng and C. H. Lu, *J. Am. Ceram. Soc.*, 2011, **94**, 2878.
30 C. H. Huang, T. M. Chen, W. R. Liu, Y. C. Chiu, Y. T. Yeh and S. M. Jang, *ACS Appl. Mater. Interfaces*, 2010, **2**, 259.
31 C. H. Huang and T. M. Chen, *J. Phys. Chem. C*, 2011, **115**, 2349.
32 G. Li, Y. Zhang, D. Geng, M. Shang, C. Peng, Z. Cheng and J. Lin, *ACS Appl. Mater. Interfaces*, 2012, **4**, 296.
33 W. J. Yang and T. M. Chen, *Appl. Phys. Lett.*, 2006, **88**, 101903.
34 K. H. Kwon, W. B. Im, H. S. Jang, H. S. Yoo and D. Y. Jeon, *Inorg. Chem.*, 2009, **48**, 11525.
35 P. I. Paulose, G. Jose, V. Thomas, N. V. Unnikrishnan and M. K. R. Warrier, *J. Phys. Chem. Solids*, 2003, **64**, 841.
36 D. L. Dexter, *J. Chem. Phys.*, 1953, **21**, 836.
37 G. Blasse, *Philips Res. Rep.*, 1969, **24**, 131.
38 D. L. Dexter and J. H. Schulman, *J. Chem. Phys.*, 1954, **22**, 1063.
39 Z. G. Xia, R. S. Liu, K. W. Huang and V. Drozd, *J. Mater. Chem.*, 2012, **22**, 15183.